Wavelet-based regularization for robust microwave imaging in medical applications

Rosa Scapaticci *Member, IEEE*, Panagiotis Kosmas *Member, IEEE*, Lorenzo Crocco *Senior Member, IEEE*

***Abstract*—Microwave imaging (MWI) is an emerging tool for medical diagnostics, potentially offering unique advantages such as the capability of providing quantitative images of the inspected tissues. This involves, however, solving a challenging non-linear and ill-posed electromagnetic inverse scattering problem. This paper presents a robust method for quantitative microwave imaging in medical applications where very little, if any, *a priori* information on the imaging scenario is available. This is accomplished by employing a distorted Born iterative method (DBIM) and a regularization by projection technique, which reconstructs the tissue parameters using a wavelet basis expansion to represent the unknown contrast. This approach is suited for any microwave medical imaging application where the requirement for increased resolution dictates the use of higher frequency data, and consequently, a robust regularization strategy. To demonstrate the robustness of the proposed approach, the paper presents reconstructions of highly heterogeneous anatomically realistic numerical breast phantoms in a canonical two-dimensional (2-D) configuration.**

***Index Terms*—electromagnetic scattering inverse problem, distorted Born inversion method, medical imaging, microwave imaging, wavelet transform.**

I. Introduction

QUANTITATIVE microwave imaging (MWI) aims at retrieving the unknown features of a target from processing measured electromagnetic (EM) field data. MWI is relevant to many applications, ranging from subsurface prospecting to biomedical monitoring, and requires the solution of a non-linear and ill-posed inverse scattering problem [1]. In medical imaging, microwave tomography has made significant progress towards clinical applications [2]. Initial clinical results have already been reported in the literature for microwave breast cancer detection [3], [4], which has arguably been the driving application for the development of both radar-based and EM inverse scattering approaches [5].

Iterative local optimization methods such as the Gauss-Newton (GN) algorithm are widely used to tackle EM inverse scattering problems, but their sensitivity to the adopted "initial guess" can be critical in applications where very little *a priori* information may be available, such as medical imaging [6]. In particular, an "initial guess" provides the starting point for these convex optimisation algorithms, and inaccurate information can lead to false solutions which fit the data but are completely different from the ground truth [7].

This paper addresses this challenge by proposing a modification of the GN optimization approach, which is implemented via the distorted Born iterative method (DBIM) [8] and is regularized by a projection of the unknown contrast function on a wavelet basis. The DBIM requires the computation of the total field inside the current estimate of the profile, which is updated at each iteration. Recent advances in highly efficient forward solvers based on graphic processor units (GPU) programming can overcome the heavy computational burden required by this numerical approach and allow its application to realistic 3-D EM inverse scattering problems, such as quantitative microwave breast imaging [9], [10].

Projecting the unknown contrast function into a representation basis is not new in EM inverse scattering; different possibilities have been suggested in biomedical applications, such as spatial Fourier harmonics [11], Gaussian basis functions [12], and wavelets [13], [14]. It is evident that the choice of the basis function will have an impact on both the efficiency (related to the number of non-zero coefficients) and the accuracy of the representation (i.e., the fidelity of the representation with respect to the actual profile). In light of this fact, the wavelet decomposition appears to be a suitable choice to tackle the typically heterogeneous scenarios occurring in medical imaging, as it allows to represent a given profile with a low number of non-zero coefficients without a significant loss of resolution (due to its intrinsic multi-resolution abilities). Moreover, the wavelet transform can capture information on both the spatial and the frequency domain, allowing significant wavelet coefficients to concentrate only in the areas of high variability where higher resolution is required.

The use of wavelets as the representation basis in EM inverse scattering has already led to good results in contrast source inversion (CSI) formulations [13], [14], but the incorporation of this method within the DBIM algorithm is examined in detail for the first time. As the DBIM solves a new linear problem at each iteration, the wavelet representation combined with the self-regularizing properties of the conjugate gradient least-squares (CGLS) method offers a flexible regularization approach that can be adjusted to take into account various parameters such as frequency range, number of iterations, residual data errors, etc. In addition, the proposed wavelet

The paper was submitted in June 2014.

This work was initiated during Rosa Scapaticci's visit at King's College London, which was supported by the COST action IC1102 through a Short Term Scientific Mission Grant. The work was developed further under the framework of COST Action TD1301, MiMed.

Rosa Scapaticci and Lorenzo Crocco are with CNR-IREA, National Research Council of Italy - Institute for Electromagnetic Sensing of the Environment, via Diocleziano 328, 80124, Napoli, Italy, e-mail: scapaticci.r@irea.cnr.it; crocco.l@irea.cnr.it.

Panagiotis Kosmas is with the School of Natural and Mathematical Sciences, King's College London, London, WC2R 2LS, U.K., e-mail: panagiotis.kosmas@kcl.ac.uk

Corresponding author: L. Crocco

implementation does not require a fixed number of steps or ad-hoc criteria for the termination of the CGLS iterative process to avoid instabilities, as in previous implementations of the method [15], [16].

The remainder of the paper is structured as follows: after reviewing the basics of the DBIM in Section II, Section III introduces the wavelet representation and discusses its effect on the developed algorithm. Section IV discuss the exploitation of frequency diversity in our inversion algorithm. Section V presents results to illustrate the advantages of this approach over conventional DBIM using anthropomorphic breast phantoms, in Section VI we report a robustness analysis of the procedure and Section VII offers some final conclusions and discussion.

II. The DBIM scheme

It is well known that the inverse EM scattering problem is non-linear and ill posed. In a DBIM scheme, the non-linearity of the inverse scattering problem is tackled through a succession of linear approximations, where the unknown is the variation of the contrast function $\Delta\chi = \varepsilon - \varepsilon^b$, which accounts for the variation between the actual permittivity profile and the one of an assumed reference "background" scenario. This latter is iteratively updated, as well as the corresponding background field inside the domain $\underline{E}^b$, which approximate the (unknown) total field $\underline{E}$ [8] .

Accordingly, denoting with $\underline{r}_T$ and $\underline{r}_R$ the position of the transmitters and receivers respectively, the scattering integral equation within the DBIM approximation is given by [1],

$$\Delta\underline{E}_s(\underline{r}_T,\underline{r}_R) = \underline{E}(\underline{r}_T,\underline{r}_R) - \underline{E}^b(\underline{r}_T,\underline{r}_R) = \\ = \omega^2\mu \int_V \underline{\underline{G}}^b(\underline{r},\underline{r}_R)\Delta\chi(\underline{r})\underline{E}^b(\underline{r},\underline{r}_T)d\underline{r} = \mathcal{L}^b[\Delta\chi] \qquad (1)$$

where $\Delta\underline{E}_s(\underline{r}_T,\underline{r}_R)$ is the scattered electric field due to the contrast variation $\Delta\chi(\underline{r})$ in the volume V with respect to the current background, and $\underline{\underline{G}}^b(\underline{r},\underline{r}_R)$ denotes the dyadic background Green's function, which represents propagation from the source located at $\underline{r} \in V$ to the point $\underline{r}_R$. The resulting linear integral equation is solved (in the discrete domain) at each iteration of the DBIM algorithm for the contrast function $\Delta\chi(\underline{r})$, and can also be represented with the use of the integral operator $\mathcal{L}^b$ in (1).

The iterative update of the reference background scenario requires updates of the field $\underline{E}^b$ and the Green's function $\underline{\underline{G}}^b$ at each iteration, which can be computed numerically from the *forward solution* of the scattering equation (1). Conversely, the inversion of the resulting linear equation represents the *inverse solution* and provides the estimate of the contrast function, which is used to update the background profile at the next iteration. This can be performed via a conjugate gradient least square (CGLS) algorithm, which involves the minimization of the quadratic cost functional $\Phi(\Delta\chi) = \|\mathcal{L}^b[\Delta\chi] - \Delta\underline{E}_s\|^2$ through an *inner* iterative procedure.

[1]In the following, as well as in next Section, the formulation is given for functions defined over a continuous domain and for the 3D vectorial problem, the reduction to the discrete 2D scalar problem, dealt with in the numerical examples, being straightforward.

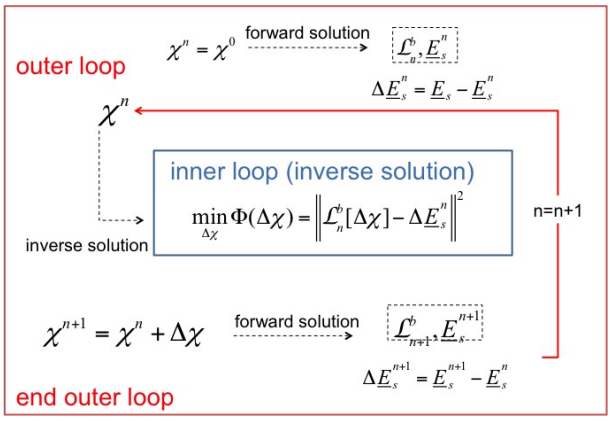

Fig. 1. A schematic representation of the DBIM algorithm.

This process can be schematically represented with two nested loops, as in Fig.1: the "outer" loop implements the linearization of (1) at each DBIM iteration, while the "inner" loop involves the inverse solution of the resulting linear system. The stopping rule for the outer loop can be dictated by a (prefixed) maximum number of given iterations or a stopping criterion based on the norm of the residual $\Delta\underline{E}_s$. The regularization of the problem comes into play independently in the inner loop only. As mentioned above, we implement the solution of the linear system in the inner loop via a Conjugate Gradient Least Square (CGLS) algorithm and apply a wavelet-based regularization by projection approach described in the next Section.

III. Wavelet-based Regularization in the DBIM

A. The use of wavelets as basis representation

A way to reduce the ill-posedness of an under-determined linear problem (and possibly reduce its computational complexity) is to represent the unknown function $\Delta\chi$ through its projection onto a finite number N of orthogonal basis functions ψ_n,

$$\Delta\chi = \sum_{n=1}^{N} x_n\psi_n. \qquad (2)$$

Under this transformation, the actual unknowns of the inverse problem are the projection coefficients $\{x_n\}_{n=1}^N$.

In this framework, the adopted basis plays a key role, as it has to be accurate and efficient. Efficiency requires a reduced number of coefficients in the representation, while accuracy involves a low representation error, which quantifies the mismatch between the actual function and its projection onto the considered basis. This paper argues that the wavelet basis is a good choice to accommodate the trade off between efficiency and accuracy of the representation. Indeed, the intrinsic multiresolution feature of the wavelet transform [17] allows an accurate representation of the unknown function with a reduced number of coefficients.

In particular, the wavelet transform decomposes a given profile into two sets of coefficients: coarse and detail. The coarse coefficients account for the profile's low frequency

content acting as a low-pass filter of the original function, while detail coefficients account for high frequency content and allow representing the finer details of the function [17]. As the decomposition level increases, the number of non-zero coefficients is reduced. These properties motivate an approach that starts from a high level of decomposition, which is gradually reduced to retrieve finer details in the image. In practice, this is achieved by starting from a high order coarse representation and progressively moving to lower order coarse images to improve resolution.

B. Wavelet-based CGLS

The regularization by projection on wavelets comes into play in the inverse solution. In particular, once the Green function $\underline{G}^b$ and the incident field $\underline{E}^b$ have been updated and the current background operator $\mathcal{L}^b$ has been constructed (outside the CGLS), we solve the linear problem which minimizes the following quadratic cost functional,

$$\Phi(\Delta\chi) = \|\mathcal{L}^b\left[\Delta\chi\right] - \Delta\underline{E}_s\|^2. \tag{3}$$

To solve this minimization problem with respect to the wavelet coefficients, we denote with W the operator which transforms $\Delta\chi$ into wavelet coefficients and with W^{-1} the inverse wavelet transforms, which operates on wavelet coefficients and returns a spatial representation. In this case, the expression of the cost functional $\Phi(\Delta\chi)$ can be rewritten as a function of $x = W(\Delta\chi)$ as follows,

$$\Phi(x) = \|\delta(x)\|^2 = \langle\delta(x), \delta(x)\rangle \tag{4}$$

wherein $\delta(x) = \{\mathcal{L}^b\left[W^{-1}(x)\right] - \Delta\underline{E}_s\}$.

In order to minimize this cost functional via a CGLS method, one has to find a gradient of the functional and a direction of descend. To pursue the first goal, it is sufficient to derive the functional Φ with respect to x, that is,

$$\frac{\partial\Phi}{\partial x} = \langle\delta(x), \mathcal{L}^b\left[W^{-1}(\Delta x)\right]\rangle + c.c. = \langle W\{(\mathcal{L}^b)^+\left[\delta(x)\right]\}, \Delta x\rangle + c.c., \tag{5}$$

wherein $^+$ denotes the Hermitian and $c.c.$ the complex conjugate. From (5) it follows that the gradient of Φ with respect to the wavelet coefficients is

$$\nabla\Phi_x = W\{(\mathcal{L}^b)^+\left[\delta(x)\right]\}. \tag{6}$$

In order to find the update direction λ, it is sufficient to calculate the functional $\Phi(x + \lambda\Delta x)$ and find λ which minimizes it, that is

$$F(\lambda) = \Phi(x + \lambda\Delta x) = a\lambda^2 + b\lambda + c \tag{7}$$

where:

$$\begin{aligned} a &= \|\mathcal{L}^b W^{-1}(\Delta x)\|^2, \\ b &= 2Re\langle\mathcal{L}^b\left[W^{-1}(\Delta x)\right], \delta(x)\rangle, \\ c &= \|\delta(x)\|^2. \end{aligned} \tag{8}$$

As can be seen from (7), the functional $F(\lambda)$ is formally the equation of a parabola with a minimum represented by its vertex.

Wavelet coefficients for the next iteration are updates as $x^{i+1} = x^i + \lambda\nabla\Phi_x$. The stopping rule for this wavelet-based CGLS (W-CGLS) is determined by the slope of the residual $R(k) = \delta(x^k)$. In particular the CGLS loop stops as soon as $R(k-1) - R(k) \leq 0.01\left(R(1) - R(2)\right)$.

IV. A HYBRID STRATEGY TO EXPLOIT FREQUENCY DIVERSITY

The use of multi-frequency data in MWI can be beneficial in terms of both robustness and resolution. In particular, frequency diversity enlarges the ratio of independent data to unknown parameters thereby reducing the occurrence of false solutions [7], [18]. We hereby discuss our approach to using multi-frequency data within the proposed algorithm.

A popular method for the use of multi-frequency data is based on frequency hopping, where single-frequency (monochromatic) reconstructions are performed successively from low to high frequencies [19]. This approach has the advantage of being very simple in handling the dispersive behavior of human tissues. Moreover, the use of low frequencies in the initial inversion stages reduces the non-linearity of the problem and acts as a "regularizer" in the later stages of the frequency hopping approach. The method, however, is computationally expensive for a DBIM algorithm and may not take full advantage of high-frequency data, as it will be inevitably biased towards the solutions provided at the low frequencies considered initially. In addition, it is worth recalling that frequency hopping does not yield an actual enlargement of the data-to-unknown ratio [18].

A second obvious possibility for exploiting multi-frequency data is to simultaneously consider all the available frequencies [15], [18], [20]–[22]. This entails the necessity of adopting a proper dispersion model throughout the inversion process, but also allows increasing the amount of exploited independent data and therefore pursuing a solution for an enlarged set of unknowns. On the other hand, the presence of high-frequency data increases the non-linearity of the problem and thus the need of a robust regularization method to avoid local minima.

To balance between these two strategies, this work considers frequency diversity by means of a *hybrid* approach similar to [18], in which a good initial guess is initially pursued by inverting monochromatic data followed by simultaneous processing of multi-frequency data. This strategy is perfectly suited with our wavelet projection approach, which aims at retrieving only a *smooth* version of the actual profile at its first steps requiring the use of lower frequencies. Conversely, the use of higher frequencies is useful to reconstruct higher resolution details after a good initial guess is obtained. At this stage, the simultaneous use of different frequencies can take advantage of the enlargement of the essential dimension of the space wherein data are represented with a beneficial effect on the ratio between data and unknowns [18].

We implement the multiple-frequency DBIM similar to [12], [15] by capturing the dependence of the dielectric properties of human tissues on frequency by a single-pole Debye model,

$$\varepsilon_r(\omega) = \varepsilon_\infty + \frac{\Delta\varepsilon}{1 + j\omega\tau} + \frac{\sigma_s}{j\omega\varepsilon_0}, \tag{9}$$

$$\begin{bmatrix} \Re\{\mathcal{L}^b(\omega_1)\} & \frac{\Re\{\mathcal{L}^b(\omega_1)\}+\omega_1\tau\Im\{\mathcal{L}^b(\omega_1)\}}{1+(\omega_1\tau)^2} & \omega_1\omega_1^{-1}\Im\{\mathcal{L}^b(\omega_1)\} \\ \Im\{\mathcal{L}^b(\omega_1)\} & \frac{\Im\{\mathcal{L}^b(\omega_1)\}-\omega_1\tau\Re\{\mathcal{L}^b(\omega_1)\}}{1+(\omega_1\tau)^2} & \omega_1\omega_1^{-1}\Re\{\mathcal{L}^b(\omega_1)\} \\ \Re\{\mathcal{L}^b(\omega_2)\} & \frac{\Re\{\mathcal{L}^b(\omega_2)\}+\omega_1\tau\Im\{\mathcal{L}^b(\omega_2)\}}{1+(\omega_2\tau)^2} & \omega_2\omega_2^{-1}\Im\{\mathcal{L}^b(\omega_2)\} \\ \Im\{\mathcal{L}^b(\omega_2)\} & \frac{\Im\{\mathcal{L}^b(\omega_2)\}-\omega_2\tau\Re\{\mathcal{L}^b(\omega_2)\}}{1+(\omega_2\tau)^2} & \omega_2\omega_2^{-1}\Re\{\mathcal{L}^b(\omega_2)\} \\ \cdot & \cdot & \cdot \\ \cdot & \cdot & \cdot \\ \cdot & \cdot & \cdot \\ \Re\{\mathcal{L}^b(\omega_F)\} & \frac{\Re\{\mathcal{L}^b(\omega_F)\}+\omega_F\tau\Im\{\mathcal{L}^b(\omega_F)\}}{1+(\omega_F\tau)^2} & \omega_F\omega_F^{-1}\Im\{\mathcal{L}^b(\omega_1)\} \\ \Im\{\mathcal{L}^b(\omega_F)\} & \frac{\Im\{\mathcal{L}^b(\omega_F)\}-\omega_1\tau\Re\{\mathcal{L}^b(\omega_F)\}}{1+(\omega_F\tau)^2} & \omega_F\omega_F^{-1}\Re\{\mathcal{L}^b(\omega_2)\} \end{bmatrix} W^{-1} \begin{bmatrix} x_\infty \\ x_\Delta \\ \frac{x_\sigma}{\varepsilon_0\omega_1} \end{bmatrix} = \begin{bmatrix} \Re\{\Delta\underline{E}_s(\omega_1)\} \\ \Im\{\Delta\underline{E}_s(\omega_1)\} \\ \Re\{\Delta\underline{E}_s(\omega_2)\} \\ \Im\{\Delta\underline{E}_s(\omega_2)\} \\ \cdot \\ \cdot \\ \cdot \\ \Re\{\Delta\underline{E}_s(\omega_1)\} \\ \Im\{\Delta\underline{E}_s(\omega_1)\} \end{bmatrix} \tag{10}$$

where ε_∞, $\Delta\varepsilon$, τ and σ_s are the Debye parameters that capture frequency dependence. Lazebnik et al. have shown that the Debye model in (9) provides an accurate representation of the frequency-dependent behavior of the dielectric properties of breast tissues at microwave frequencies [23]. The relaxation time τ can be considered known and constant, which allows a linear model for the three other unknown parameters in (9). This is a reasonable assumption since τ does not vary extensively across different biological tissues [23], [24].

The multi-frequency approach involves solving (1) at multiple discrete frequencies, say F. To this end, the system of equations at different frequencies are coupled via the Debye model such that the contrast function $\Delta\chi$ represents the contrast of the unknown parameters of the model. Since the model parameters take real values, the first step is to separate the real and imaginary components of each set of equations. Then, the real and imaginary part of the contrast is expressed in terms of the Debye parameters, obtaining the set of equations in (10).

The vector of unknowns x is constituted by three subvectors x_∞, x_Δ and x_σ, which contain the wavelet coefficients obtained by projecting the contrast functions χ_∞, χ_Δ and χ_σ of corresponding Debye parameters ε_∞, $\Delta\varepsilon$ and σ_s. The solution of (10) is formally equivalent to that described above, once the metrics and the vector of the unknowns have been properly redefined. In particular, we can use the symbol M to refer to the matrix on the left-hand side of (10), X for the vector of the unknowns and b for the right-hand side of (10) (representing the data of the problem), so that the equation to be inverted at each of the DBIM iteration is in the form $MW^{-1}(X) = b$.

V. Numerical analysis

To assess the performance of the proposed inversion approach in microwave medical imaging applications with little *a priori* information, we have considered two-dimensional (2-D) anthropomorphic breast phantoms taken from University of Wisconsin at Madison's numerical repository [25]. To construct 2-D phantoms, we have extracted a slice and performed a resizing of the original grid so that the actual cell dimension is equal to 2.0 mm. We consider two breast phantoms belonging to different classes: slice $s_1 = 112$ from phantom ID 062204 representing a heterogeneously dense breast, and slice $s_1 = 65$ from phantom ID 012304 corresponding to a very dense breast. We assume that these phantoms are immersed in a lossless coupling medium having relative permittivity of $\varepsilon_b = 18$, as suggested in [11]. In practice, mixtures of vegetable oil and water can be used to achieve these permittivity values with very low losses in the considered frequency range ($1 - 3$ GHz) [26].

The adopted measurement configuration considers 16 filamentary sources surrounding the breast at positions with average distance of approximately 1 cm from the skin layer. This number of antennas is chosen as a trade-off between the system's complexity and the need to gather as much independent information as possible. According to theoretical considerations [27], [28], this number suffices to collect all the available information at the lowest frequency of 1 GHz considered here in a non-redundant way, but corresponds to undersampled data at the higher frequencies. This motivates our hybrid frequency diversity approach further, as it allows an "initial guess" reconstruction based on accurately sampled low-frequency data (at 1 GHz).

We simulate measured data using the Finite-Difference-Time-Domain (FDTD) method and a uniform grid cell size of 2.0 mm, which is also used as the forward solver in the inversion process. The Debye parameters for the various tissues are extracted from UW-Madison's repository data [25]. The simulated data have been corrupted with additive Gaussian noise with SNR of 60 dB relative to the energy of total field, i.e., the field computed in presence of the phantom. Note that, the projection of the unknown on a representation basis, as well as the presence of noise on data assure that no "inverse crime" is committed.

In the reconstructions below, the only *a priori* assumption used in the initial guess of the DBIM algorithm is the knowledge of the actual shape of the breast. This is a reasonable assumption for many practical cases, such as in systems where the breast is hosted into a cup (of course the presence of such a cup should then be taken into account in the inversion process) or where complementary methods are used to estimate the breast surface [29]. The starting guess assumes that the actual shape is filled with homogeneous fatty tissue ($\varepsilon_\infty = 5.76$, $\Delta\varepsilon = 5.51$ and $\sigma_s = 0.0802$ S/m). The Debye parameter τ is fixed for all breast tissues equal to 17.5ps. We note that these initial values are considerably lower than the true average Debye parameters for these dense breast phantoms, which were required for previous conventional DBIM-

CGLS algorithms to converge [15], [16]. Finally, the inversion scheme constrains the reconstructed Debye parameters within a reasonable range belonging to breast tissue suggested by the experimental observations in [23], i.e., $\varepsilon_\infty \in [4.68 - 25]$, $\Delta\varepsilon \in [3.12 - 52]$ and $\sigma_s \in [0.0697 - 0.9]$ S/m.

Based on our frequency diversity strategy, the first step of the procedure has been carried out by inverting monochromatic data at a frequency of 1 GHz. In this step, the multiresolution feature of wavelets has been explored by changing the decomposition level of the Discrete Wavelet Transform (DWT) throughout the iterations. In particular we performed 5 iterations for a 3^{rd} level decomposition, the next 5 iterations at the 2^{nd} decomposition level and finally 5 iterations at the 1^{st} level of decomposition. Then the second step has been carried out by inverting multifrequency data at eleven frequencies evenly spaced in the range $1 - 3$ GHz. A 1^{st} level per 10 iterations and a 0^{th} level (which is equivalent to considering a pixel representation) per 20 iterations have been adopted in this second step. The mother wavelet adopted during the procedure is the Daubechies20.

The accuracy of the obtained reconstructions is quantified by means of the root mean square reconstruction error (RMSE):

$$\text{RMSE} = \frac{\|\varepsilon - \tilde{\varepsilon}\|^2}{\|\varepsilon\|^2}, \tag{11}$$

ε and $\tilde{\varepsilon}$ being the the reference complex permittivity and the reconstructed one, respectively.

Moreover, in order to easily connect the reconstruction error to the "quality" of the achieved result, we also report the RMSE, computed separately for the real and imaginary part of the complex permittivity (which are actually the parameters shown in next figures.

$$\text{RMSE}_{\varepsilon'} = \frac{\|\varepsilon' - \tilde{\varepsilon}'\|^2}{\|\varepsilon'\|^2}, \tag{12a}$$

$$\text{RMSE}_{\varepsilon''} = \frac{\|\varepsilon'' - \tilde{\varepsilon}''\|^2}{\|\varepsilon''\|^2}, \tag{12b}$$

ε' and ε'' being the real part and imaginary part of the reference complex permittivity and $\tilde{\varepsilon}'$, $\tilde{\varepsilon}''$ the reconstructed ones.

The obtained reconstructions of the permittivity profile at 1 GHz (at the end of the first step of the inversion process) and at 3 GHz (after second step) are shown in Figs.2 - 3 for the two phantoms, which clearly show that both the morphology and the microwave properties of the imaged breast have been accurately retrieved. Reconstruction errors are reported in Table I. To test robustness, we have repeated the reconstructions for an initial breast model filled with a homogeneous fibroglandular tissue ($\varepsilon_\infty = 14.00$, $\Delta\varepsilon = 30.12$ and $\sigma_s = 0.7$ S/m). The resulting reconstruction for the very dense breast is shown in Fig.4, which clearly suggests that the algorithm is robust with respect to *a priori* information on the interior of the breast. The reconstruction errors in this case are RMSE$= 0.28$, $\text{RMSE}_{\varepsilon'} = 0.29$ and $\text{RMSE}_{\varepsilon''} = 0.58$.

TABLE I
RECONSTRUCTION ERROR

	$f = 1$ GHz			$f = 3$ GHz		
RMSE	on ε	on ε'	on ε''	on ε	on ε'	on ε''
Heterog. dense breast	0.41	0.45	0.88	0.28	0.28	0.53
Very dense breast	0.39	0.38	0.97	0.29	0.27	0.50

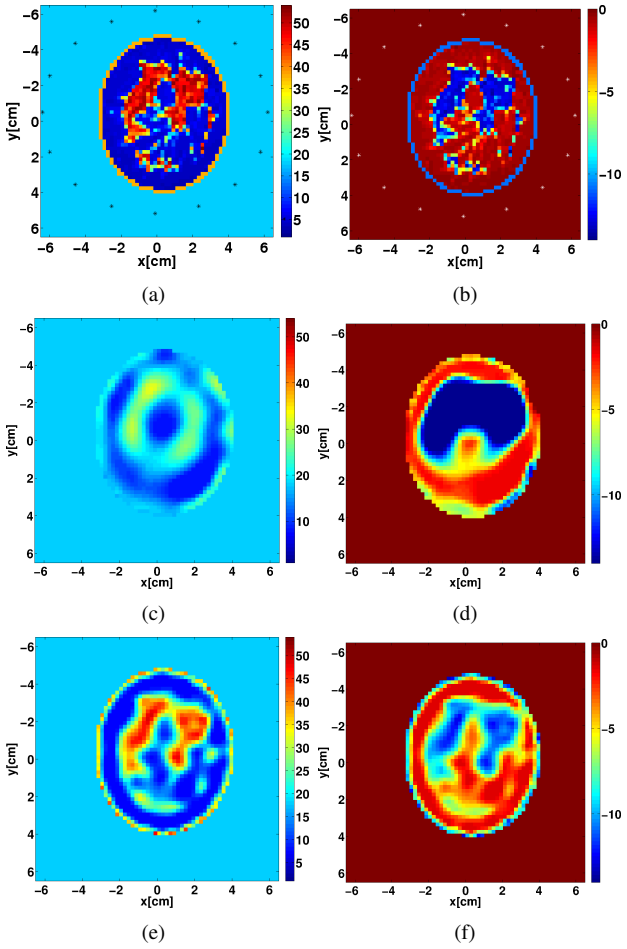

Fig. 2. Heterogeneously dense breast. (a) Real part ε' and (b) imaginary part ε'' of the reference permittivity profile; (c) Real part ε' (d) imaginary part ε'' recovered from the monochromatic processing at 1 GHz;(e) Real part ε' (f) imaginary part ε'' at 3 GHz recovered at the end of the procedure.

VI. Robustness Analysis

A. Impact of using multi-frequency data

To illustrate the advantage of using the proposed hybrid approach for multi-frequency data, we have tested the other two approaches discussed in Section III-C (frequency hopping and single-step simultaneous multi-frequency reconstruction) for the heterogeneously dense breast phantom of Fig.2(a)-(b). Corresponding reconstructions of the relative permittivity are shown in Fig.5. It is evident that simultaneous multi-frequency reconstructions lead to a completely unreliable result. Conversely, the frequency hopping procedure returns a good reconstruction, but some finer details lost as suggested also by a slightly higher reconstruction error (RMSE$= 0.28$, $\text{RMSE}_{\varepsilon'} = 0.29$, $\text{RMSE}_{\varepsilon''} = 1.54$). The frequency hopping procedure, however, is much more demanding from a computational point of view, as it requires to perform F sequential

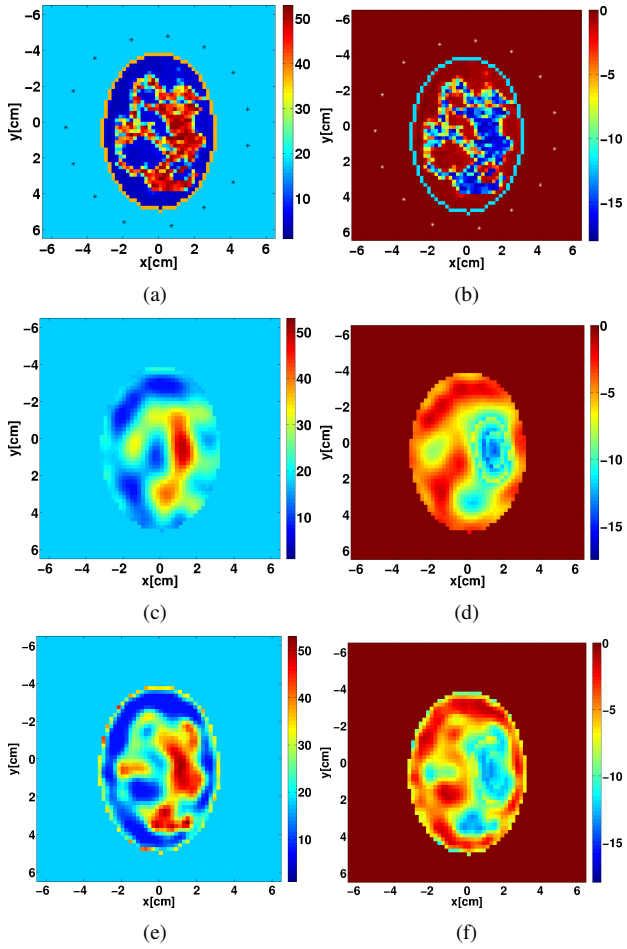

Fig. 3. Very dense breast. (a) Real part ε' and (b) imaginary part ε'' of the reference permittivity profile; (c) Real part ε' (d) imaginary part ε'' recovered from the monochromatic processing at 1 GHz;(e) Real part ε' (f) imaginary part ε'' at 3 GHz recovered at the end of the procedure.

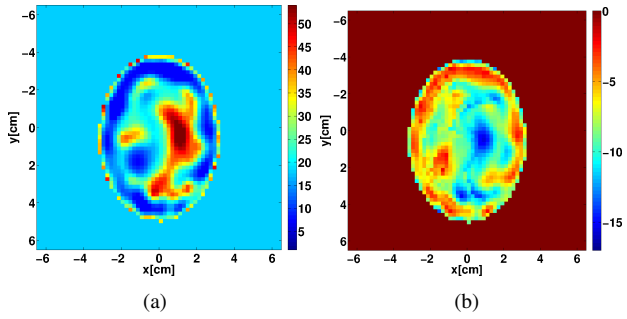

Fig. 4. Effect of the assumed average tissue value. Reconstructions of the permittivity profile of a very dense breast obtained starting from a homogeneous brest having the average electric properties of fibroglandular tissue. (a)Relative permittivity and (b) ε''.

DBIM reconstructions, with F equal to the number of involved frequencies.

B. Impact of the regularization by projection approach

As mentioned previously, the proposed wavelet projection's regularizing properties increase the robustness of the DBIM algorithm with respect to the initial guess. Indeed, we have tested the DBIM algorithm using a conventional CGLS implementation with an ad-hoc stopping criterion in the inner loop of Fig.1 and verified that it does not converge to a meaningful solution for the "fatty tissue initial guess", which is considerably lower than the average properties for these dense breast phantoms. This is illustrated in Fig.6 for the very dense breast of Fig.3(a)-(b). The reconstruction in this case is completely unreliable and the procedure is trapped in a false solution even when using low-frequency data at 1 GHz.

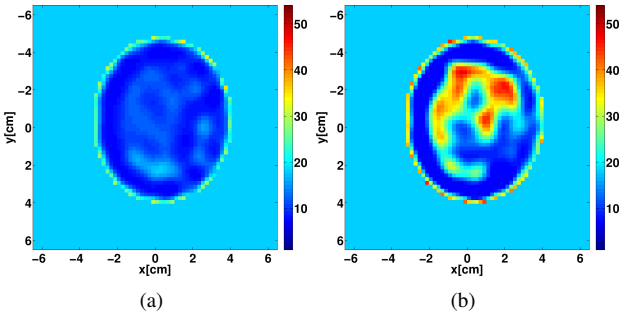

Fig. 5. Results for different strategies for the use of multi-frequency data. Heterogeneously dense breast - Reconstructions of the real part ε' (at 3 GHz) obtained by means of (a) simultaneous multi-frequency processing and (b) a frequency hopping procedure.

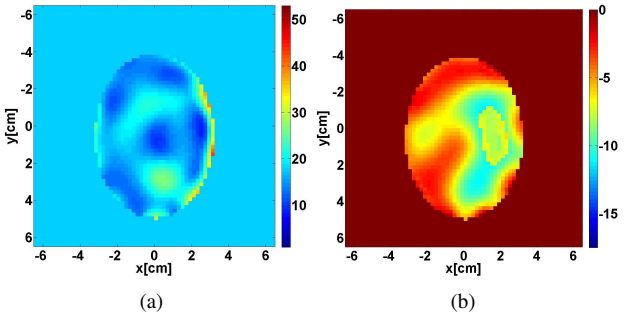

Fig. 6. Effect of the regularization by projection on wavelets. Very dense breast - Reconstructions of the complex permittivity profile without regularization recovered from the monochromatic processing at 1 GHz. (a) Real part ε' and (b) imaginary part ε''.

VII. Conclusion

This paper presents a novel inversion approach for quantitative microwave medical imaging, which employs the wavelet transform as a means of regularization for the inverse EM scattering problem encountered in microwave tomography. We have argued that wavelets allow for an efficient representation of the unknown contrast, leading to a reduced number of coefficients with minimal information loss. We have presented an inversion process that exhibits two innovative features: first, the adoption of a regularization by projection on wavelets in a DBIM scheme, and second, a hybrid approach in the exploitation of multi-frequency data. We have assessed the algorithm's performance by reconstructing dense 2-D anthropomorphic breast phantoms characterized by different percentage of fibroglandular/adipose tissues.

Our results have demonstrated the increased robustness of our wavelet-based CGLS method over traditional CGLS approaches. Moreover, our method does not require any explicit regularization schemes that can be computationally demanding

and compromise resolution. It also offers additional flexibility, as the number of elements for the representation basis can be reduced for frequencies under 1 GHz and increased as we move towards higher frequencies. However in this work we have considered 1 GHz as starting point as a trade-off between spatial resolution of the first achieved estimate and its reliability.

The computational time needed to achieve a reconstruction like the ones showed in this paper is about one hour, running non optimized codes on a standard computer, having 8 GB RAM and two 2.17 GHz processors. We are currently extending the proposed algorithm to a fully 3-D implementation, which will be presented in future work, and, once optimized, it is expected to return a reconstruction in the order of some hours, that can be considered clinically reasonable.

Finally, similar to all other MWI techniques applied to breast cancer, the ability of a clinical MWI system based on this approach to detect cancerous tissue will depend on the tumor size and location. In particular, detecting very small tumors would require the use of high frequency data and a high dynamic range available by the MWI apparatus. In addition, while dielectric spectroscopy data in [23] suggests that the contrast of cancerous to fibroglandular tissue is considerably lower than that of cancerous to adipose tissue, very recent clinical studies [31], have shown that an increase of the conductivity at lower frequency (i.e., below 2 GHz) can be considered as a marker of tumor aggressiveness. This suggests that successful tumor detection by microwave tomography requires accurate quantitative estimation of both the real and imaginary parts of the tissue complex permittivity, which can be indeed achieved by our method.

REFERENCES

[1] D. Colton and R. Kress, "Inverse acoustic and electromagnetic scattering theory", 2nd ed Springer, Berlin, 1998.

[2] S. Semenov, "Microwave tomography: Review of the progress towards clinical applications," *Phil. Trans. R. Soc. A*, vol. 367, pp. 3021-3042, 2009.

[3] P. M. Meaney, M. W. Fanning, T. Raynolds, C. J. Fox, Q. Q. Fang, C. A. Kogel, S. P. Poplack, and K. D. Paulsen, "Initial clinical experience with microwave breast imaging in women with normal mammography," *Acad. Radiol.*, vol. 14, no. 2, pp. 207-218, Feb. 2007.

[4] Fear, J. Bourqui, C. Curtis, D. Mew, B. Docktor, and C. Romano, "Microwave breast imaging with a monostatic radar-based system: a study of application to patients, *IEEE Trans. Microw. Theory Tech.*, vol. 61, no. 5, pp. 2119-2128, May 2013.

[5] N. K. Nikolova, "Microwave imaging for breast cancer," *IEEE Microwave Mag.*, vol. 12, no. 7, pp. 78-94, 2011.

[6] T. M. Grzegorczyk, P. M. Meaney, P. A. Kaufman, R. M. di Florio-Alexander, and K. D. Paulsen, "Fast 3-D tomographic microwave imaging for breast cancer detection," *IEEE Tran. on Med. Imaging*, vol. 31, no. 8, pp. 1584-1592, Aug. 2012.

[7] T. Isernia, V. Pascazio, and R. Pierri, "On the local minima in a tomographic imaging technique", *IEEE Trans Geosci. Rem. Sens.*, vol. 39, pp. 1596-1607, 2001.

[8] W. C. Chew and Y. M.Wang, "Reconstruction of two-dimensional permittivity distribution using the distorted born iterative method," *IEEE Trans. Medical Imag.*, vol. 9, pp. 218-225, 1990.

[9] J.D. Shea, P. Kosmas, B.D. Van Veen, and S.C. Hagness,"Contrast enhanced microwave imaging of breast tumors: A computational study using 3D realistic numerical phantoms", *Inv. Prob.*, vol.26, no.7, pp.1-22, Jun. 2010.

[10] H. Zhou, T. Takenaka, J. E. Johnson, and T. Tanaka ,"A breast imaging model using microwaves and a time domain three dimensional reconstruction method, *Progress in Eletromagnetic Research*, Vol.93, pp. 57-70, 2009.

[11] I. Catapano, L. Di Donato, L. Crocco, O.M. Bucci, A.F. Morabito, T. Isernia, and R. Massa, "On quantitative microwave tomography of female breast", *Progress In Electromagnetic Research*, PIER 97, pp.75-93, 2009.

[12] D.W. Winters, J.D. Shea, P. Kosmas, B.D. Van Veen, and S. C. Hagness, "Three-dimensional microwave breast imaging: Dispersive dielectric properties estimation using patient-specific basis functions", *IEEE Trans. on Medical Imaging*, vol.28, no. 7, pp.969-981, 2009.

[13] R. Scapaticci, I. Catapano, and L. Crocco, "Wavelet-based adaptive multiresolution inversion for quantitative microwave imaging of breast tissues", *IEEE Trans. on Antennas and Propagat.*, vol. 60, no.8, pp. 3717-3726, 2012.

[14] M. Li, O. Semerci, and A. Abubakar, "A contrast source inversion in the wavelet domain", *Inverse Problems*., vol. 29(2), 025015(19pp), 2013.

[15] J. D. Shea, P. Kosmas, S. C. Hagness, and B. D. Van Veen, "Three-dimensional microwave imaging of realistic numerical breast phantoms via a multiple-frequency inverse scattering technique," *Med. Phys.*, vol. 37, no. 8, pp. 4210-4226, Aug. 2010.

[16] P. Kosmas, J. D. Shea, B. D. Van Veen, and S. C. Hagness, "Three-dimensional microwave imaging of realistic breast phantoms via an inexact Gauss-Newton algorithm," *in 2008 IEEE Internat. Symp. Antennas Propag.*, pp. 1-4, July 2008.

[17] S.G. Mallat, "A theory for multiresolution signal decomposition: the wavelet representation", *IEEE Trans. Pattern Anal. Machine Intell.*, vol.2, no.7, pp.674-693, 1989.

[18] O.M. Bucci, L. Crocco, T. Isernia, and V. Pascazio, "Inverse scattering problems with multifrequency data: reconstruction capabilities and solution strategies",*IEEE Trans. Geosci. Remote Sens.*, vol.38, pp.1749-1756, 2000.

[19] W.C. Chew and J.H. Lin, "A frequency-hopping approach for microwave imaging of large inhomogeneous bodies", *IEEE Microwave and Guided Wave Letters*, vol.5, pp.439-441,2002.

[20] P.D. Jensen, T. Rubaek, and J.J. Mohr, "Utilization of multiple frequencies in 3D nonlinear microwave imaging," *Proc. of 6th European Conference on Antennas and Propagation (EUCAP 2012)*, Prague (CZ), pp. 1776-1779, 2012.

[21] K. Belkebir, R.E. Kleinman, and C. Pichot, "Microwave imaging-Location and shape reconstruction from multifrequency scattering data," *IEEE Trans. Microwave Theory and Tech.*, vol.45, no.4, pp. 469-476, 1997.

[22] A. Fhager, M. Gustafsson, S. Nordebo, "Image reconstruction in microwave tomography using a dielectric Debye model, *IEEE Trans. Biomedical Engineering*, vol. 59 , no. 1, pp. 156-166, 2012.

[23] M. Lazebnik, D. Popovic, L. Mc Cartney, C.B. Watkins, M.J. Lindstrom, J. Harter, S. Sewall, T. Ogilvie, A. Magliocco, T.M. Breslin, W. Temple, D. Mew, J.H. Booske, M. Okoniewski, and S.C. Hagness, "A large-scale study of the ultrawideband microwave dielectric properties of normal, benign and malignant breast tissue obtained from cancer surgeries", *Phys. Med. Biol.*, vol.52, pp.6093-6115, 2007.

[24] S.Gabriel, R.W.Lau and C.Gabriel,"The dielectric properties of biological tissues: III. Parametric models for the dielectric spectrum of tissues," *Phys. Med. Biol.*, vol.41, pp. 2271-2293, 1996.

[25] E. Zastrow, S.K. Davis, M. Lazebnik, F. Kelcz, B.D. Van Veem, and S.C. Hagness, "Database of 3D Grid-Based Numerical Breast Phantom for use in Computational Electromagnetics Simulations", *IEEE Trans. Biomed. Eng.*,vol. 55, no.12, pp. 2792-2800, 2008.

[26] J. Stang, M. Haynes, P. Carson and M. Moghaddam, "A Preclinical System Prototype for Focused Microwave Thermal Therapy of the Breast", *IEEE Trans. Biomedical Engineering*, vol. 59, pp. 2431-2438, 2012.

[27] O.M. Bucci, G. Franceschetti, "On the degrees of freedom of scattered fields", *IEEE Trans. Antennas Propag.*, vol.37, pp.918926, 1989.

[28] O.M. Bucci, T. Isernia, "Electromagnetic inverse scattering: retrievable information and measurement strategies", *Radio Science*, vol.32, pp.2123-2138, 1997.

[29] T. C. Williams, J. Bourqui, T. R. Cameron, M. Okoniewski, and E. C. Fear, "Laser surface estimation for microwave breast imaging systems," *IEEE Trans. Biomedical Engineering*, vol. 58, no. 5, pp. 11931199, 2011.

[30] T. Rubk, Paul M. Meaney, and Keith D. Paulsen, "A Contrast Source Inversion Algorithm Formulated Using the Log-Phase Formulation," *International Journal of Antennas and Propagation*, vol. 2011, Article ID 849894, 10 pages, 2011. doi:10.1155/2011/849894

[31] P. M. Meaney, A. P. Gregory, N. R. Epstein and K. D. Paulsen, "Microwave open-ended coaxial dielectric probe: interpretation of the sensing volume re-visited", *BMC Medical Physics*, vol.14(3), 2014.

Rosa Scapaticci was born in Naples, Italy, in 1985. In March 2010, she received the master degree (summa cum laude) in Biomedical Engineering from the ”Federico II” University of Naples and in May 2014 she received the Ph.D. degree in Information Engineering from the ”Mediterranea” University of Reggio Calabria. Since December 2013, she is a Research Fellow at the Institute of Electromagnetic Sensing of the Environment, National Research Council of Italy (IREA-CNR), Naples. The scientific interests of Dr. Scapaticci are mainly focused on the development of innovative approaches for the solution of electromagnetic scattering problems, particularly in the framework of biomedical microwave imaging, and therapeutic applications of electromagnetic fields. In 2013, Dr. Scapaticci has been awarded by IEEE - Antennas and Propagation Society Central and Southern Italy Chapter for the best Student Member paper, while in September 2014 she received the Barzilai Award from the Italian Society of Electromagnetics.

P. Kosmas , Senior Member IEEE 2013, joined King’s College London (KCL) as a Lecturer in 2008, and is currently a member of KCL’s Centre for Telecommunications (CTR) within the Department of Informatics. Prior to his appointment, he held research positions at the Center for Subsurface Sensing and Imaging Systems, Boston, USA, the University of Loughborough, UK, and the Computational Electromagnetics Group, University of Wisconsin-Madison, USA. His expertise in microwave imaging includes radar and tomographic methods, and he has pioneered the use of time reversal for microwave breast cancer detection. He has over 50 journal and conference publications on microwave imaging and related areas. He is also the co-founder of Mediwise Ltd, a UK-based SME focusing on the use of EM waves for medical applications. Beyond microwave medical imaging, Dr Kosmas’ research interests include computational electromagnetics with application to other areas of subsurface sensing, antenna design, and inverse problems theory and techniques.

Lorenzo Crocco (Naples, Italy, 1971) received the Laurea degree (summa cum laude) in electronic engineering and the Ph.D. degree in applied electromagnetics from the University of Naples ”Federico II”, in 1995 and 2000, respectively. Since 2001, he has been a Research Scientist with the Institute for the Electromagnetic Sensing of the Environment, National Research Council of Italy (IREA-CNR), Naples. In 2009-2011, he was adjunct professor at the Mediterranea University of Reggio Calabria (Italy), where he currently is a member of the Board of Ph.D. advisors. His scientific interests include electromagnetic scattering problems, imaging methods for noninvasive diagnostics, through the wall radar and ground-penetrating radar, as well as microwave biomedical imaging and therapeutic uses of electromagnetic fields. With respect to these topics, Lorenzo Crocco has published more than 60 papers on peer reviewed international journals, given keynote talks at international conferences and lead or actively contributed to Italian and European research projects. Moreover, he has served as Guest Editor for international scientific journals. Currently, he is member of the management committee of COST Action TD1301 on microwave medical imaging. Dr. Crocco is a Fellow of The Electromagnetics Academy (TEA). He was the recipient of the ”Barzilai” Award for Young Scientists from the Italian Electromagnetic Society (2004) and Young Scientist Awardee at the XXVIII URSI General Assembly (2005). In 2009, he was awarded as one of the top one-hundred under 40 scientists of CNR.